Surface structures of In-Pd intermetallic compounds. II. A theoretical study

Émilie Gaudry, Garry Mcguirk, Julian Ledieu, Vincent Fournée

Surface structures of In-Pd intermetallic compounds. II. A theoretical study

É. Gaudry, G. M. McGuirk, J. Ledieu, and V. Fournée
Institut Jean Lamour, Université de Lorraine CNRS UMR 7198, Parc de Saurupt, 54011 Nancy Cedex, France

The (110) surface of the InPd intermetallic compound and the In–Pd surface alloy properties are investigated in the framework of the density functional theory, within the projector augmented plane-wave method. Surface segregation is calculated to be energetically unfavorable at stoichiometric InPd(110) surfaces, while indium antisites are shown to segregate to the surface in off-stoichiometric InPd(110) systems. Concerning surface alloys obtained by burying In-doped Pd layers in Pd(111), we demonstrated that the most stable ones are those presenting atomic indium concentrations below 50 at. % (11 at. %, 25 at. %, 33 at. %). According to our calculations, the In-doped Pd layers with concentration above or equal to 50% lead to In-doped Pd multilayers, each presenting an atomic indium concentration below 50 at. %. Alloying and segregation effects in InPd intermetallic compound and In–Pd surface alloys clearly agree with the larger bonding strength of In–Pd (-0.44 eV) compared to In–In (-0.29 eV) and Pd–Pd (-0.31 eV). © *2014 AIP Publishing LLC.* [http://dx.doi.org/10.1063/1.4892409]

I. INTRODUCTION

In a context where fossil fuels are becoming increasingly costly, the development of new clean sources of energy is awaited. A few years ago, Olah suggested to use methanol to store energy and to produce convenient hydrocarbon-based fuels and products.[1,2] Among other advantages, methanol possesses high potential as hydrogen carrier[3–5] and methanol steam reforming (MSR) is a promising reaction to release hydrogen. Indeed, it represents the chemical reaction with the highest hydrogen concentration in the gas products ($CH_3OH + H_2O \rightarrow 3H_2 + CO_2$). Selectivity in this reaction is crucial: the complete methanol decomposition ($CH_3OH \rightarrow 2H_2 + CO$) produces CO, which is poisonous, at concentrations above 20 ppm, to the Pt-electrode in the proton exchange membrane fuel cells.[6,7] Hence, the choice of the catalyst is of great importance to reach a high conversion rate and selectivity, while still preserving a long-term stability. Copper-based catalysts are the most commonly used materials. However, these types of catalysts are pyrophoric and deactivated by thermal sintering. Pd and Pt catalysts, usually supported on oxide supports like ZnO or In_2O_3, also present high performances towards MSR. The intermetallic compounds (ZnPd, ZnPt, or InPd) formed during the reaction by partial reduction of the supporting oxide, are frequently observed, and are supposed to play a role in the reactivity.[8–13] In particular, their electronic structures exhibit a valence electron density of state similar to pure Cu.[13,14]

The rational design and optimization of active and selective MSR catalysts require the understanding of the reaction mechanism at an atomic scale on model systems. The knowledge of the surface structure is a prerequisite for such studies. Experimentally, surface investigations under ultra-high vacuum are usually realized using single crystals. When sizable single crystals are not available, it is also possible to use surface alloys for surface science studies, by evaporating metals in vacuum onto metal surfaces. In the latter case, intermix-ing at the atomic scale may occur during deposition, or can be induced by successive thermal treatments.[15] In the case of Zn–Pd surface alloys, the deposition of Zn on a Pd(111) surface leads experimentally to various structures, depending on the Zn coverage.[16,17] A $p(2 \times 1)$ surface structure has been identified for a Zn coverage between 0.8 ML and 1.5 ML, by an approach combining both experimental and theoretical results.[17] Calculations based on Monte Carlo simulations highlight the dependence of the surface structure on the Zn coverage. For one or more layer of Zn deposited on Pd(111), a multilayer 1:1 Zn–Pd surface alloy is formed, while surface alloy islands dominated by Pd are shown to be formed at sub-monolayer Zn coverage.[18] The resulting structure of surface alloys highly depends on preparation conditions. Indeed, in such systems, the balance between the alloying effect and the surface segregation dictates the surface structure. Theoretical calculations are essential to analyze in details the experimental observations and to understand the segregation trends in a system.[19–21] Multiscale segregation simulations can also provide a prediction of the temperature-dependent alloy composition at the surface.[22]

The present paper aims to bring a deeper understanding of the experimental results obtained for the In/Pd(111) system reported in Ref. 23. It is also the basis for a theoretical analysis of the InPd(110) surface and of indium segregation in Pd(111). The paper is organized as follows. We first provide computational details in Sec. II. The results are presented in Sec. III for bulk systems (Pd, In, InPd, and In_7Pd_3), for the InPd(110) surface and for In–Pd surface alloys. The results are discussed in terms of bonding strengths and in the light of an experimental study of In/Pd(111)[23] (Sec. IV) before we conclude.

II. METHOD

Calculations are performed using the Vienna *ab initio* Simulation Package (VASP) based on the Density

Functional Theory (DFT).[24,25] The interaction between the valence electrons and the ionic core is described using the projector-augmented wave (PAW) method.[26,27] The electronic exchange and correlation contribution is described using the generalized gradient approximation GGA-PBE.[28,29] Geometries are optimized by the calculation of the Hellmann-Feynman forces acting on atoms and their minimization via a conjugate gradient algorithm (forces on moving atoms are less than 0.02 eV/Å). The parameters linked to the numerical implementation of the DFT, i.e., the plane-wave cutoff E_{cut} and the density of k-points sampling the Brillouin zone, were converged by means of a series of test calculations to ensure the same energy precision in all calculations (less than 1 meV), leading to the following values: E_{cut} (450 eV) and σ = 0.2 eV. The k-points grid was set to 23 × 23 × 23 for bulk InPd (2 at./cell), as well as for bulk Pd and bulk In. For other geometries, the k-points grid was set to reach the same precision. Surfaces are modeled by slabs separated by a 15 Å void thickness.

The surface energy of the InPd(110) surface is calculated in Sec. III B 1. A common method for calculating surface energies γ for simple metal surfaces is based on the difference between the total energy $E_{surf}(N\text{layers})$ of a symmetric N-layer thick slab (1 atom per layer) and the one of the corresponding bulk (E_{bulk}, expressed in eV/at.)

$$\gamma = \frac{E_{surf}(N\text{layers}) - N E_{bulk}}{2A}, \quad (1)$$

where A is the surface area of the unit cell. The factor $\frac{1}{2}$ accounts for the two surfaces of the slab model. This equation is still valid for a stoichiometric surface, where the slab model is built by a stacking of planes with a chemical composition identical to the bulk composition. Usually, the computation of the total energy of a series of slabs of different thickness is used to extract the surface energy from Eq. (1), to prevent surface energies divergence as a function of the slab thickness.[30,31] More recently, Da Silva *et al.*[32] have shown that the surface energy, computed from Eq. (1) with slab and total energies obtained from separate DFT calculations, converges as a function of the number of layers in the slab, providing that both calculations are carried out with the same high accuracy.

III. RESULTS

A. Bulk structures and cohesive energies

The bulk cell parameters and cohesive energies of Pd, In, InPd, and In$_7$Pd$_3$ are summarized in Table I. Our PAW calculations are in overall agreement with experimental data. Our calculated equilibrium lattice parameters of *bct* indium and *fcc* palladium are 1%-2% larger than those deduced from experiments, while the one calculated within the local density approximation scheme are found to be 1%-2% smaller.[33] This is in agreement with the usual LDA over-binding and GGA over-corrections. Concerning bulk Pd, our PAW-PBE calculations are also in agreement with previously published all electron calculations,[32] justifying the use of time-saving pseudopotentials rather than all electron potentials.

TABLE I. Bulk lattice parameters and cohesive energies E_c of Pd, In, InPd, and In$_7$Pd$_3$.

	Latt. param. (Å)		E_c (eV/at.)	
	Exp.	Calc.	Exp.	Calc.
Pd	3.884[34]	3.94	−3.94[35]	−3.77
		3.85 (LDA)[32,33]		−5.04 (LDA)[32]
		3.95 (PBE)[32,36]		−3.68 (PBE)[36]
				−3.65 (PBE)[32]
In	$a = 3.256$[37]	$a = 3.31$	−2.52[35]	−2.35
	$c = 4.940$[37]	$c = 5.03$		
		$a = 3.18$ (LDA)[33]		
		$c = 4.89$ (LDA)[33]		
InPd	3.25[38]	3.30	…	−3.57
In$_7$Pd$_3$	9.4359[37]	9.59	…	−3.18

In this paper, the surface energy of InPd(110) is evaluated, along with segregation energies for the In/Pd(111) system. This requires the determination, as a first step, of the In$_x$Pd$_{1-x}$ mixing enthalpy and the dilute impurity enthalpy. The calculation of these quantities are detailed in the following.

The mixing enthalpy per atom, ΔH_m, for the In$_x$Pd$_{1-x}$ solid solution is defined by

$$\Delta H_m = E_c(\text{In}_x\text{Pd}_{1-x}) - (1-x)E_c(\text{Pd}) - x E_c(\text{In}), \quad (2)$$

where $E_c(\text{In}_x\text{Pd}_{1-x})$ is the cohesive energy per atom of the solid solution, $E_c(\text{Pd})$ and $E_c(\text{In})$ are the cohesive energies per atom of the pure Pd and In phases. For the stoichiometric InPd and In$_7$Pd$_3$ compounds ($x = 0.5$ and $x = 0.7$, respectively), the mixing enthalpy is also known as the formation enthalpy ΔH_f. We found $\Delta H_f(\text{InPd}) = -0.51$ eV/at. and $\Delta H_f(\text{In}_7\text{Pd}_3) = -0.40$ eV/at., to be compared to the experimental values $\Delta H_f(\text{InPd}) = -0.65$ eV/at.[39] and $\Delta H_f(\text{In}_7\text{Pd}_3) = -0.45$ eV/at.[40] measured at $\simeq$300 K. The mixing enthalpy ΔH_m was also calculated in the dilute In limit, by considering a 3 × 3 × 3 *fcc*-Pd supercell, containing $N = 108$ atoms, where one Pd atom was substituted by one In atom

$$N\Delta H_m\left(x = \tfrac{1}{N}\right) = E[(N-1)\text{Pd, In}]$$
$$- \tfrac{N-1}{N}E[N\text{Pd}] - \tfrac{1}{N}E[N\text{In}]. \quad (3)$$

We find $\Delta H_m(0.92\%) = -18$ meV/at. Negative mixing enthalpies at $T = 0$ K, as presently obtained in the dilute limit, means that the alloy will form a solid solution in the absence of any competing ordered phase. We also checked the stability of the In$_x$Pd$_{1-x}$ alloy, with $x = 0.92\%$, against a demixion in pure Pd and the ordered InPd$_2$ phase by evaluating the energy difference $E[(N-1)\text{Pd, In}] - E[\text{InPd}_2] - (N-3)E[\text{Pd}]$ (−3 meV/at.). The stability against the demixion in pure Pd and InPd$_3$ has not been evaluated, since this compound contains some disorder.[41]

The mixing enthalpy can then be expressed as a function of the dilute impurity enthalpy per In atom ΔH_{imp}

$$\Delta H_m(x) = x\Delta H_{imp}, \quad (4)$$

where the dilute impurity enthalpy per In atom is defined by

$$\Delta H_{imp} = \lim_{x \to 0} \left(\frac{1}{x} \Delta H_m(x) \right)$$

$$= \mu_{In}(x \to 0) - \mu_{In}(x \to 1)$$

$$= \mu_{In}(x \to 0) - E_c(In). \tag{5}$$

In the previous equation, $\mu_{In}(x)$ is the chemical potential or partial enthalpy per atom of In in the In–Pd alloy at concentration x. We found $\Delta H_{imp} = -1.91$ eV/at. and $\mu_{In}(x \to 0) = -4.26$ eV.

B. InPd(110) surface

1. Surface energy

The surface energy of the non-relaxed (110) surface has been evaluated by a linear regression on the total energy of different slabs built with an increased number of planes. For a symmetric slab built with n atomic layers, the non-relaxed surface energy $\gamma_{(110)}^{non-relax}$ is given by

$$E_n^{tot} = 2\gamma_{(110)}^{non-relax} A_{(110)} + 2n E_c^{InPd}, \tag{6}$$

where E_n^{tot} is the total energy of the slab, $A_{(110)}$ is the area of the surface unit cell (15.40 Å^2), and E_c^{InPd} is the cohesive energy of InPd. The surface energy of the unrelaxed system has been derived from fitting E_n^{tot} in various ranges, $n = 8 - 12$, $n = 9 - 12$, $n = 10 - 12$, leading to $\gamma_{(110)}^{non-relax} = 0.82$ J/m^2 within $\simeq 10$ mJ/m^2. The fitting procedure also leads to $E_c^{InPd} = -3.57$ eV/at., whatever is the range chosen for n, in good agreement with the value deduced from a direct calculation (Table I, $E_c^{InPd} = -3.57$ eV/at.).

The same procedure can be applied with an asymmetric slab (5 fixed planes and $n - 5$ planes allowed to relax). A similar equation as above was used to determine the surface energy

$$E_n^{tot} = \gamma_{(110)}^{non-relax} A_{(110)} + \gamma_{(110)}^{relax} A_{(110)} + 2n E_c^{InPd}, \tag{7}$$

where $\gamma_{(110)}^{relax}$ is the relaxed surface energy. The fitting procedure ($n = 8 - 12$) gives $\gamma_{(110)}^{relax} = 0.72$ J/m^2 and we check that the value found for E_c^{InPd} (-3.57 eV) is again in good agreement with the previous values. The relaxation energy of the surface is then evaluated to be equal to 0.10 J/m^2 (more than 10%), which is quite high compared to simple metals. In this latter case, the variation of the surface energy due to relaxation is typically of the order of 2%-5%.[42–44] Here, the relaxation energy of the InPd(110) surface is related to atomic relaxations (see Sec. III B 2).

2. Atomic relaxations

The relative interlayer relaxations $\Delta_{\ell,\ell-1}$, defined by

$$\Delta_{\ell,\ell-1} = \frac{(d_{\ell,\ell-1} - d_{bulk})}{d_{bulk}}, \tag{8}$$

where $d_{\ell,\ell-1}$ is the interlayer spacing between layers ℓ and $\ell - 1$ are small: $\Delta_{S,S-1} = 0.02$ at the surface and decreases rapidly for subsurface layers. The corrugation χ^ℓ of

the atomic plane ℓ, defined by

$$\chi^\ell = z^\ell(In) - z^\ell(Pd) \tag{9}$$

is non-negligible for the first two layers: $\chi^S = 0.26$ Å, $\chi^{S-1} = 0.12$ Å, while $\chi^\ell < 0.02$ Å for $\ell = S - 3, S - 4$, etc. The Pd atom moves slightly inward, with respect to its position in the unrelaxed slab while the In atom moves slightly outward. This result can be rationalized by the smaller surface energy of In compared to Pd: $\gamma_{Pd(111)}^{fcc} = 2.05$ J/m^2 and $\gamma_{In(001)}^{bct} = 0.675$ J/m^2.[45] This behavior is very similar to what occurs on the stoichiometric ZnPd surface.[14]

3. Electronic structure

We discuss here the electronic structure of the InPd(110) surface. Indeed, the valence d states of this surface are of particular importance for the surface reactivity, which is the ultimate target of the present investigation of alloy catalyst.

The electronic structure of bulk InPd is represented in Fig. 1 (bottom), highlighting the similarity in the valence electron DOS for InPd and pure Cu, except near the Fermi energy ($[E_F - 1.5 \text{ V}; E_F]$). The electronic structure of the InPd(110) surface is also represented in Fig. 1. The surface
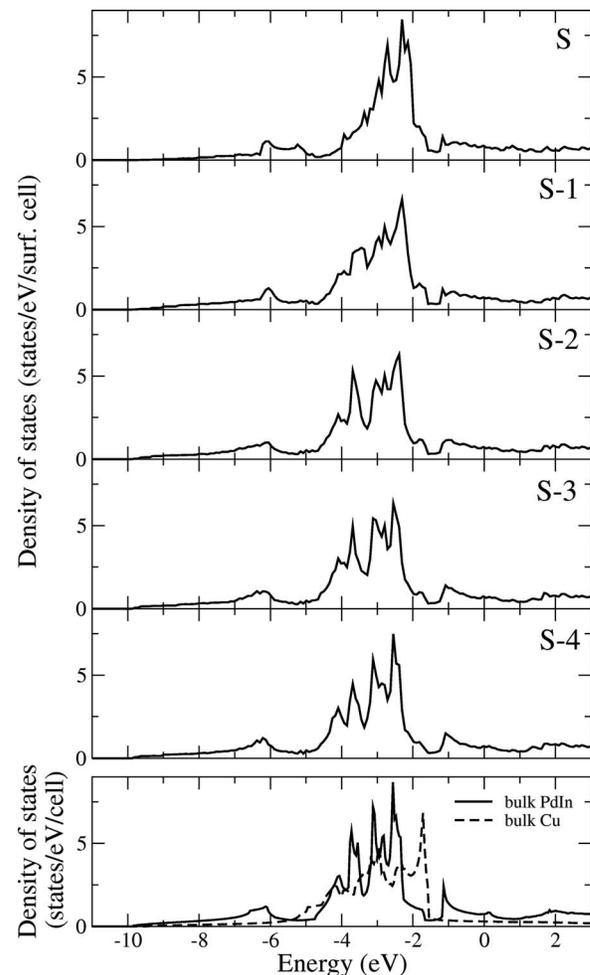

FIG. 1. Electronic structure of the InPd(110) surface, showing the contributions of the different atomic layers. The electronic structure of bulk Cu and InPd are given for comparison.

contribution of the *d*-band is narrower and shifted ($\simeq 0.45$ eV) towards the Fermi energy compared to the bulk one. The same occurs in the subsurface layer, to a lesser extent. Within the Friedel's model, where the density of states of the *d*-band is modeled by a rectangular shape, these results can be rationalized as follows. Since the width of the band depends on the hybridization of neighboring atomic orbitals (the higher the coordination, the more overlap and the broader the band is), and since the whole material has a single Fermi energy, the reduced coordination of the surface atoms leads to a narrowing and a shift of the valence *d*-band (the shift aims to avoid an unrealistic lack or excess on electronic charge on the surface atoms).[46]

4. Indium surface segregation in InPd

In Secs. III B 1–III B 3, we considered a perfect bulk terminated InPd(110). In simple alloys, it is well known that surface segregation often occurs. Here, we give first results concerning segregation at InPd(110) surface.

Indium segregation at the InPd(110) surface is evaluated by comparing the relative formation energies for a bilayer of pure In or In-doped Pd deposited on the InPd(110). The relative formation energy $\Delta E_f(c_S, c_{S-1})$ of a surface bilayer with In concentration (c_S, c_{S-1}) in the surface and subsurface layers, respectively, is defined by

$$\Delta E_f(c_S, c_{S-1}) = E_{slab}(c_S, c_{S-1}) - E_{slab}(50\%, 50\%), \quad (10)$$

where $E_{slab}(c_S, c_{S-1})$ is the total energy of a slab with a surface bilayer of composition (c_S, c_{S-1}). We found $\Delta E_f(100\%, 0\%) = 0.78$ eV and $\Delta E_f(75\%, 25\%) = 0.37$ eV. The positive value for ΔE_f indicates that indium segregation is not energetically favorable, due to the quite large energy required to break In–Pd bonds.

In the previous paragraph, we considered a perfect InPd intermetallic compound. According to the phase diagram, the existence of cubic InPd ranges from 45 at. % Pd to 61.5 at. % Pd. The constitutional point defects are identified to be Pd vacancies (In-rich alloys) and Pd antisites (Pd-rich alloys) by first principles calculations.[33] The presence of such defects can modify strongly the In segregation pattern.[47–49] To investigate the influence of the composition on surface segregation, we have compared the total energies of slabs containing one point defect either in surface or in "bulklike" layer (position $S - 4$). The surface cell dimensions are 4.67×6.60 Å^2 (1×2) and the shortest distance between two points defects due to periodic conditions is 4.67 Å. This distance might be a little too short to avoid any interactions between defects. However, these possible interactions exist both for defects in the surface and "bulklike" atomic layers. We then expect that these interactions are negligible when calculating relative energies. Results gathered in Table II highlight a large negative value for In antisites, and positive values for other defects. According to these results, In antisites are expected to segregate to the InPd(110) surface, while other defects are supposed to stay in the bulk. In the case of Pd antisites, this can be understood with the relatively high surface energy of Pd(111) ($\gamma_{Pd(111)}^{fcc} = 2.05$ J/m^2).[45] Concerning vacancies, the calculated stabilization energies are small ($\delta E \simeq 0.1$ eV). The present

TABLE II. Energy difference $\Delta E = E_{surf}(x) - E_{bulklike}(x)$ between the surface and bulklike defects in off-stoichiometric InPd intermetallic compounds.

	Pd-rich		In-rich	
	Pd antisite	In vacancy	Pd vacancy	In antisite
Comp. (Pd at. %)	52.1	51.1	48.9	47.9
ΔE (eV)	0.74	0.09	0.14	-1.35

calculations cannot exclude in this case a contribution from interaction between vacancies.

C. Indium surface segregation in Pd(111)

The segregation of indium at the (111) surface of Pd was studied systematically by burying a layer with different indium concentrations into a Pd(111) crystal. The considered asymmetric slabs consist of 13 layers: 12 pure Pd layers (6 fixed at the bottom and 6 allowed to relax) and one layer containing In, allowed to relax. The Pd(111) slab is thick enough to bury the In-doped Pd layer in the first five surface planes. The layer by layer surface segregation study evaluates the total energy of a slab, built by substituting an increasing number of Pd atoms in a given Pd layer ℓ. The In concentration in layer ℓ has been varied from the almost dilute limit (1/9) up to a complete In monolayer. The segregation energy per In atom, with In layer concentration c in surface layer ℓ, is defined as the energy gained, by indium atom when a concentration c of In atoms are transferred from a bulk layer to that of the surface layer[44]

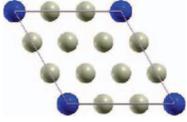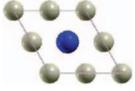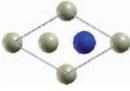$$E_{seg}(c, \ell) = \frac{E_{slab}(c, \ell, x) - \lim_{\ell' \to \infty} E_{slab}(c, \ell', x)}{c}, \quad (11)$$

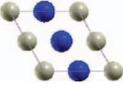where $E_{slab}(c, \ell, x)$ is the energy of a semi-infinite Pd$_{1-x}$In$_x$ alloy with an indium concentration c in layer ℓ. When ℓ tends to infinity, $E_{seg}(c, \ell)$ tends to zero.

In this paper, we considered only ordered phases, for which the mixing entropy is small.[50] We should emphasise here that the number of configurations investigated is obviously limited by the size of the unit cell, so that only highly ordered structures can be simulated. Other structures besides those explicitly considered here could have lower energies, and disordered structures could play a role as well. These problems are typically dealt with, in alloy simulations, using a cluster expansion approach.[51] This latter approach is beyond the scope of the present paper.

1. Single indium-doped layer buried in Pd(111)

In this section, we study the stability of a single In-doped Pd layer buried in Pd(111) with concentrations from 11% to 100% at. In. The considered systems correspond to different ordered alloys with a In-doped layer structure shown in Table III. For the three lower In concentrations (11%, 25%, 33%, first raw of Table III), the In atoms of the In-doped Pd plane are surrounded only by Pd atoms, the distance between two nearest neighbors In atoms being equal to 3, 2, and $\sqrt{3}$

TABLE III. Structure of the planes containing In buried in Pd(111). Blue spheres (resp. gray spheres) represent In atoms (resp. Pd atoms). c is the concentration of the In-doped Pd plane. The nearest neighbors (NN) of In and Pd atoms, in the considered In-doped Pd plane, are detailed for each system, along with the ratio d_{ij}/d, where d_{ij} is the nearest neighbor distances In–In, In–Pd, and Pd–Pd and d is the calculated nearest neighbor distance in bulk Pd (2.79 Å).

c	11%	25%	33%
surf. cell	3×3	2×2	$\sqrt{3} \times \sqrt{3}$
In NN	6 Pd	6 Pd	6 Pd
Pd NN	5.25 Pd + 0.75 In	4 Pd + 2 In	3 Pd + 3 In
$d_{\text{In–In}}/d$	3	2	$\sqrt{3}$
$d_{\text{Pd–In}}/d$	1	1	1
$d_{\text{Pd–Pd}}/d$	1	1	1
c	50%	67%	100%
surf. cell	2×2	$\sqrt{3} \times \sqrt{3}$	1×1
In NN	4 Pd + 2 In	3 Pd + 3 In	6 In
Pd NN	2 Pd + 4 In	6 In	…
$d_{\text{In–In}}/d$	1	1	1
$d_{\text{Pd–In}}/d$	1	1	…
$d_{\text{Pd–Pd}}/d$	1	$\sqrt{3}$	…

times the nearest neighbor distance in Pd ($d = 2.79$ Å). For higher In concentrations, interatomic In–In distances equal to d occurs. In the case of In-doped Pd layer with In concentration equal to 67%, Pd atoms are surrounded by 6 In atoms. Interestingly, in the case of In-doped Pd layer with In concentration equal to 50%, In atoms are located in the center of a rectangle, in a similar way compared to the (110) surface. However, the dimensions of these two rectangles are not exactly the same: $\sqrt{3}d \times d$ (4.83 × 2.79 Å^2) for the In-doped Pd layer with In concentration equal to 50% and $\sqrt{2}a \times a$ (4.67 × 3.30 Å^2), where a is the cell parameter of bulk InPd, for the InPd(110) surface.

The evolution of the segregation energy with the position ℓ clearly shows that the surface S layer, and to a lesser extent the subsurface $S - 1$ layer, is a highly favorable position with negative segregation energy. The segregation energies for positions $S - 2$ and $S - 3$ is almost zero, and can then be assimilated to the bulk one ($S - 4$) within the uncertainty of the calculation. The surface segregation energy is lower for the In-rich layers, i.e., 67% and 100% and higher for the In-poor layers, i.e., 11%, 25%, and 33% (Table IV). The 50% concentration represents an intermediate case.

TABLE IV. Surface segregation energies.

c	11%	25%	33%	50%	67%	100%
$E_{seg}(c, S)$ (eV)	−0.30	−0.28	−0.28	−0.23	−0.18	−0.16

The introduction of indium in the Pd(111) substrate leads to atomic relaxations. It is worth noticing that while the layer relaxation is very weak in the dilute In limit (less than 1%), it can reach relatively high values for systems with a plane containing 100% In atomic concentration. In this latter case, if the indium plane is located at the surface, the relative interlayer relaxation $\Delta_{S, S-1}$ is 3.7%. Again, when In is located at the surface, it lies slightly above the mean position of the plane ($\simeq 0.1$ Å in the dilute limit).

In the dilute limit, the surface segregation energy is usually decomposed into three independent contributions. The main contribution comes from the differences in surfaces energies, giving the nature of the segregating species in 95% of bimetallic systems.[21] This contribution favors the segregation at the surface of the element with the lowest surface energy, which, in our case, is indium. The elastic energy contribution, proportional to the difference in elastic strain energy between the layer and the bulk, is due to the solute-solvent atomic size mismatch. In the dilute limit, within the elasticity theory, it always favors the segregation of the solute atoms at the surface, hence the surface segregation of indium in our case.[21,44] The ordering contribution depends on the alloy composition.[21] For a system presenting a tendency to bulk ordering, which is the case of InPd, the alloying term favors segregation of the majority element (Pd in this case). Given our results, this latter contribution is certainly small here.

2. Indium-doped Pd(111) multilayers

The previous stabilization energies are lower for the most highly In-doped Pd layers. Then, the question arises about the possibility for the In-doped Pd layer to transform into In-doped Pd multilayers. In the following, we evaluate this possibility as a function of both the concentration of the In-doped Pd layer and the thickness of the multilayers.

The influence of the concentration of the In-doped Pd plane on the previous process is evaluated by comparing the total energy of a surface or subsurface In-doped Pd single layer with the total energy of a surface In-doped Pd bilayer (each layer with the concentration $c/2$). It appears that the formation of a bilayer is favorable for all considered concentrations (100%, 67%, 50%), and even more favorable for a pure indium surface layer on Pd(111) (see Table V).

The next step aims to evaluate the thickness of the multilayer formed during the previous process. We calculated then the energy differences between the total energy of a n-layer thick In-doped Pd(111) system and a pure indium surface

TABLE V. Influence of surface or subsurface indium concentration (c) on the formation of a In-doped Pd surface bilayer. The table contains the energy differences (eV/ In at.) between the total energy of a single layer and a bilayer: $E_{2layers}(c/2) - E_{1layer}(c, \ell)$. For a pure indium layer, the energy difference corresponds to a mean value.

Position of	Indium concentration (%)		
the single layer	50	67	100
S	−0.34	−0.65	−1.02
S−1	−0.43	−0.70	−1.11

TABLE VI. Influence of the thickness of the multilayer formed from the splitting of a pure indium surface layer on Pd(111). The table contains the energy differences (eV/ In at.) between the total energy of a *n*-layer thick In-doped Pd(111) system and a pure indium surface layer on Pd(111).

Nb. of planes	1	2	3	4
ΔE (eV/In. at.)	0.00	-1.00	-1.49	-1.51

layer on Pd(111). The number of configurations of a *n*-layer thick In-doped Pd slab increases rapidly with *n*. In the case of bilayers, we considered the two possible configurations, leading to the conclusion that the energy difference between two configurations is smaller than 50 meV, i.e., well below the previous energy difference ($\simeq -1$ eV). In the following, only one configuration is considered for a given *n* ($n \in \{1; 4\}$). From Table VI, it appears that the transformation of a pure surface In layer into *n*-layer thick In-doped Pd layers is favorable, whatever is $n \in \{1; 4\}$. The transformation is especially favorable energetically when the In concentration in the multilayer reaches a value below 50% (25% or 33%). For these two concentrations (*c* equal to 25% or 33%), the corresponding formation energy of a single layer

$$E_f = E_{slab}(c) - E_{slab}(0) + E_c(Pd) - \mu_{In}(x \to 0), \quad (12)$$

where $E_{slab}(c)$ is the energy of the Pd(111) slab containing one In-doped surface layer (*c* In at. conc.) is negative, which is not the case for In-doped layers at higher concentrations.

3. Electronic structures

Finally, we discuss the electronic structure of few surface alloys. Surface DOS are calculated for the first two surface atomic layers of the relaxed slabs (Fig. 2). The surface electronic structure of pure indium monolayer film on Pd(111) is very similar to the one of pure Pd, with a large band ($\simeq 5$ eV),
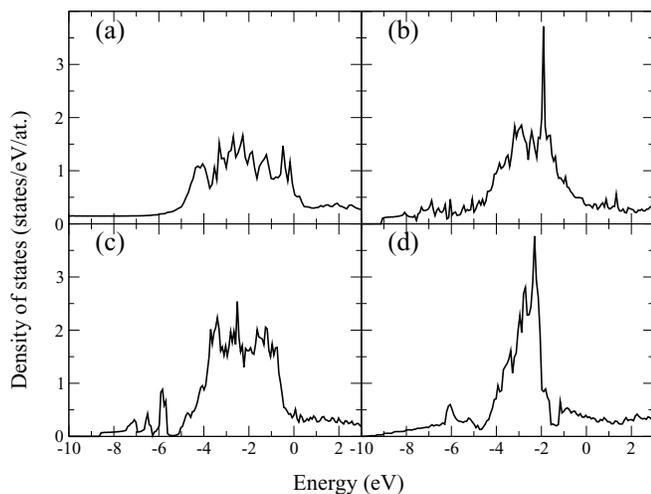

FIG. 2. Contribution of the surface bilayer (S and S−1) to the density of states of surface alloys on Pd(111) (a)–(c) and InPd(110) (d). (a) The surface layer is a pure indium layer while the subsurface layers are pure Pd layers. (b) The surface and subsurface are In-doped Pd layers, each with 50% In at. composition. This 2-layer thick film is deposited on Pd(111). (c) The surface, subsurface, and subsubsurface are In-doped Pd layers, each with 33% In at. composition. This 3-layer thick film is deposited on Pd(111).

due to a strong contribution of Pd *d*-states (Fig. 2(a)). A shift of this band towards lower energies (higher binding energies), along with a decrease of the band width, is noticeable for the other two surface alloys (33% and 50% In at. concentration per In-doped Pd layer, Figs. 2(b) and 2(c)), which tends to give a shape for these DOS similar to the one of InPd(110). However, even the 1:1 In-Pd surface alloy DOS (Fig. 2(b)) is quite different from the InPd(110) alloy (Fig. 2(d)). These results are very similar with the ones obtained from an experimental approach (Fig. 4 of Ref. 23).

Comparing in more details the InPd(110) surface DOS with the one of the 1:1 In–Pd bilayer film on Pd(111) (Figs. 2(b) and 2(d)) leads to the conclusion that the main band of the surface alloy is shifted towards the Fermi energy and broaden compared to InPd(110). As mentioned before, the environments of surface Pd and In atoms in Pd(110) and in the 1:1 bilayer film on Pd(111) are similar: each In atom lies in a rectangle made of Pd atoms. However, the dimensions do not match exactly, leading to larger atomic relaxations in the 1:1 alloy film on Pd(111) compared to InPd(110). Since the *d*-band width is inversely proportional to the third to fifth power of the distance between atoms,[52,53] the band width of InPd(110) is expected to be smaller than the one of the surface alloy: nearest neighbor In–Pd distances are equal to 2.79 Å in the surface alloy, while they are 2.86 Å in InPd(110).

IV. DISCUSSION

A. Surface alloying and segregation

Results from first-principles calculations indicate that surface alloying takes place upon In dosing on the Pd(111) surface. This behavior is due to the quite large exothermic alloy formation energy. At an atomic scale, it means that the energy gain by forming Pd–In bonds is sufficient to overcome the indium surface segregation.

The In–In, Pd–Pd, and Pd–In bonding energies can be evaluated from a simple model based on the nearest-neighbor approximation and calculated cohesive energy (Sec. III A). There are 8 nearest neighbors around each indium atom in the bulk, the In–In bonding energy is then calculated to be $E_{In\text{-}In} = -0.29$ eV. A similar reasoning leads to $E_{Pd\text{-}Pd} = -0.31$ eV, in good agreement with Ref. 54 (12 nearest neighbors around each palladium atom in the bulk) and $E_{Pd\text{-}In} = -0.44$ eV (the coordination number of each In atom in InPd is 8). The energy change due to the formation of one Pd–In bond from Pd–Pd and In–In bond is $E_{Pd-In} - \frac{1}{2}(E_{In-In} + E_{Pd-Pd})$ (-0.14 eV). Surface alloying can then be attributed to the exothermic formation energy of Pd–In bonds, since forming Pd–In bonds is energetically more favorable than forming Pd–Pd and/or In–In bonds. The alloying effect has been shown to be more favorable for In-doped Pd layers with low In concentration (11 at. %, 25 at. %, and 33 at. %). In this case, the number of Pd–In bonds is maximized within one In-doped Pd layer, each In atom being surrounded by 6 Pd atoms. In addition, the *d*-bands calculated for these surface alloys (Figs. 2(b) and 2(c)) are shifted towards lower energy (higher binding energy) compared to the surface alloy built from one pure In layer on Pd(111) (Fig. 2(a)), supporting the idea that stronger Pd–In

bonds result in a stabilization of the surface alloy. The shift is even larger for InPd(110) (Fig. 2(d)), for which the Pd–In bond is stronger.

The exothermic formation energy of Pd–In bonds is also related to the absence of surface segregation calculated in perfect InPd(110) (Sec. III B 4). Here, the suppressed surface segregation is due to the large energy required to break Pd–In bonds compared to Pd–Pd and In–In bonds. This behavior is very similar to the absence of segregation calculated for perfect 1:1 Zn–Pd alloy,[54] also due to the exothermic Pd–Zn bond formation energy (-0.13 eV). It is worth noticing that this absence of surface segregation holds only for perfect 1:1 samples: off-stoichiometric defects like In antisites are shown to segregate to the surface (Sec. III B 4). In the same way, in Zn–Pd films with 1:3 and 3:1 composition, an enrichment of the dominant component has been predicted from *ab initio* calculations.[54] This result can be related to the lower number of Pd–In or Pd–Zn bonds in such off-stoichiometric samples compared to a stoichiometric InPd intermetallic compound.

The previous results concerning segregation have been calculated for a clean surface, i.e., without taking into account the possible role of adsorbates. However, it is well known that segregation strongly depends on the surface environment. In particular, the presence of oxygen may invert the segregation profile. While in the absence of oxygen, the element with the lowest surface energy is usually exposed, the element with the highest affinity with oxygen generally segregates to the surface. This has been demonstrated for the Ag$_3$Pd alloy[55] and for the Ag–Cu[56] and Pt–Ru systems.[57] In the case of InPd, the element with the lowest surface energy (indium) is probably also the element with the highest affinity to oxygen ($\Delta G_f(\text{In}_2\text{O}_3) = -926.4$ kJ/mol and $\Delta G_f(\text{PdO}) = -115.6$ kJ/mol). Here, possible modifications of the InPd segregation profile upon adsorption is left to future work.

B. Comparison with experimental observations

The present study aims to bring a deeper understanding of the experimental results reported in Ref. 23.

Experimentally, a well-ordered phase of $(\sqrt{3} \times \sqrt{3})R30°$ is observed for low indium coverage ($\simeq 1$ MLE, i.e., 1 monolayer equivalent) after annealing, with an indium surface atomic concentration equal roughly to 30-40 at. %. This is in good agreement with the theoretical study, that shows the higher stability of a three-layer thick film (In at. % = 33%) on Pd(111) compared to a pure In monolayer on Pd(111), the stabilization energy being roughly equal to 1.5 eV/In atom.

At higher In coverage (4–35 MLE) on Pd(111), surface alloying is observed after room temperature deposition. Annealing the sample leads to the formation of two different structures depending on the annealing temperature T_a: a In$_7$Pd$_3$ surface alloy with (110) orientation ($T_a \leq 500$ K) and a InPd surface alloy with (110) orientation ($T_a = 550$–600 K). From the experimental study, the In-rich phase grows either directly on top of the Pd(111) substrate or on top of InPd(110) domains formed as an interfacial layer in the early stage of the growth. The present theoretical study shows that the energetically favorable surface alloys contain less than 50% In
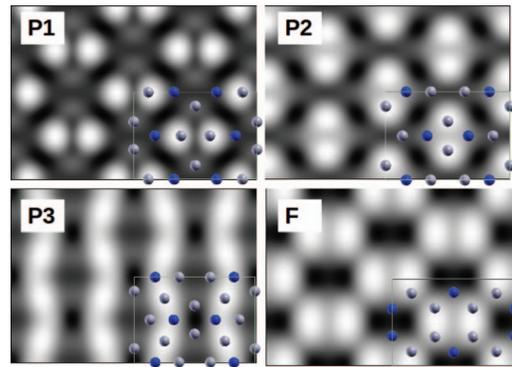

FIG. 3. Simulated STM images ($V_{bias} = +0.5$ eV, 27.1×19.8 Å^2) of possible surface terminations of the In$_7$Pd$_3$(100) surface. Blue spheres (resp. gray spheres) represent Pd atoms (resp. In atoms).

at. concentration. This conclusion is in agreement with the experimental observations, indicating that the InPd(110) and In$_7$Pd$_3$(110) surface alloys are metastable, as annealing to temperatures higher than 600 K leads to surface alloys with an indium concentration roughly equal to 20%.

The orientation of the 1:1 In–Pd surface alloy obtained experimentally has been determined from the observation of scanning tunnelling microscopy (STM) images. Alternating bright and dark rows on STM images are attributed to alternating atomic rows of Pd and In in the stoichiometric (110) atomic layers of InPd, assuming an outward shift of In atoms and an inward shift of Pd atoms, similar to what was calculated on the stoichiometric ZnPd surface.[58] The present theoretical study confirms the expected surface buckling, with an inward shift of surface Pd atoms ($\Delta z^S(\text{Pd}) = -0.10$ Å) and an outward shift of surface In atoms ($\Delta z^S(\text{In}) = 0.15$ Å).

The structure model of the In$_7$Pd$_3$(110) surface alloy assumes a bulk termination at a dense puckered layer.[23] Possible surface terminations of In$_7$Pd$_3$(110), including both puckered (P1, P2, P3) and flat (F) topmost layers, have been modelled. The corresponding STM images have been simulated within the Tersoff-Hamann approximation. Results are presented in Fig. 3. The best agreement between the simulated and the experimental image (Fig. 8(c) in Ref. 23) is obtained for the P1 termination. However, differences in the relative brightness of features are noticeable between the simulated and experimental images. Indeed, the simulation assumes a bulk termination at a dense puckered layer of In$_7$Pd$_3$(110), without taking into account the role of the substrate. A more detailed study would be required here to fully interpret the experimental observations, which is beyond the scope of this paper.

Finally, calculated density of states show that the *d*-band of In–Pd surface alloys are shifted away from the Fermi energy compared to a pure In layer on Pd(111), highlighting the alloying effect. The corresponding electronic structure is still not identical to the one of a perfect InPd(110) surface. Here, the Pd(111) surface lattice parameters have been kept fixed during atomic relaxation, leading to Pd–In bonds in the surface alloy shorter (2.79 Å) than in the stoichiometric InPd (2.86 Å). That could affect the shape and the position of the *d*-band. However, it still suggests that a sufficient thickness is required to recover the "Cu-like" electronic structure of

stoichiometric InPd. This conclusion is in line with what was calculated for the Zn/Pd(111) system:[58] the electronic structure of the Zn layers deposited on a Pd(111) substrate was found to approach the bulk Zn state only after a 4-layer thick film of Zn.

V. CONCLUSION

In this paper, we presented a detailed density functional theory study of the surface structure and the alloying and segregation effects of both the InPd intermetallic compound and In–Pd surface alloys obtained by burying a In-doped Pd layer in Pd(111).

Calculations show that segregation is energetically unfavorable at the perfect InPd(110) surface, while In antisites tend to segregate to the surface in off-stoichiometric InPd(110) systems.

Surface alloys are studied by burying an In-doped Pd layer of various compositions in Pd(111). We demonstrated that the most favorable atomic In concentrations of the In-doped Pd layer are below 50 at. % (11 at. %, 25 at. %, 33 at. %). Then, the 1:1 In–Pd surface alloy on Pd(111), obtained experimentally in Ref. [23], is not expected to be stable at the thermodynamic equilibrium. According to our calculations, the In-doped Pd layers with concentration above or equal to 50 at. % tend to transform to In-doped Pd multilayers, each presenting an atomic In concentration below 50 at. %.

Finally, the electronic structure of both InPd(110) and In/Pd(111) are investigated, suggesting that a relatively thick surface alloy is required to recover the "Cu-like" electronic structure, which is a necessary condition for the catalytic properties of InPd towards the methanol steam reforming. From the experimental and theoretical point of view, these two companion papers lay the foundations for further studies of surface reactivity.

ACKNOWLEDGMENTS

[1] G. A. Olah, "Beyond oil and gas: The methanol economy," Angew. Chem., Int. Ed. **44**, 2636–2639 (2005).

[2] G. A. Olah, A. Goeppert, and G. K. Surya-Prakash, *Beyond Oil and Gas: The Methanol Economy* (Wiley-VCH, Berlin, 2009).

[3] B. Lindström and L. J. Pettersson, "Hydrogen generation by steam reforming of methanol over copper-based catalysts for fuel cell applications," Int. J. Hydrogen Energy **26**, 923 (2001).

[4] R. M. Navarro, M. A. Pena, and J. L. G. Fierro, "Hydrogen production reactions from carbon feedstocks: Fossils fuels and biomass," Chem. Rev. **107**, 3952 (2007).

[5] D. R. Palo, R. A. Dagle, and J. D. Holladay, "Methanol steam reforming for hydrogen production," Chem. Rev. **107**, 3992 (2007).

[6] K. Narusawa, M. Hayashida, Y. Kamiya, H. Roppongi, D. Kurashima, and K. Wakabayashi, "Deterioration in fuel cell performance resulting from hydrogen fuel containing impurities: Poisoning effects by CO, CH_4, HCHO and HCOOH," JSAE Rev. **24**, 41 (2003).

[7] X. Cheng, Z. Shi, N. Glass, L. Zhang, J. Zhang, D. Song, Z.-S. Liu, H. Wang, and J. Shen, "A review of PEM hydrogen fuel cell contamination: Impacts, mechanisms, and mitigation," J. Power Sources **165**, 739 (2007).

[8] N. Iwasa, S. Masuda, N. Ogawa, and N. Takezawa, "Steam reforming of methanol over Pd/ZnO: Effect of the formation of PdZn alloys upon the reaction," Appl. Catal. A **125**, 145 (1995).

[9] N. Iwasa, T. Mayanagi, N. Ogawa, K. Sakata, and N. Takezawa, "New catalytic functions of PdZn, PdGa, PdIn, PtZn, PtGa and PtIn alloys in the conversions of methanol," Catal. Lett. **54**, 119–123 (1998).

[10] N. Iwasa and N. Takezawa, "New supported Pd and Pt alloy catalysts for steam reforming and dehydrogenation of methanol," Top. Catal. **22**, 215 (2003).

[11] Y. Men, G. Kolb, R. Zapf, M. O'Connell, and A. Ziogas, "Methanol steam reforming over bimetallic Pd-In/Al_2O_3 catalysts in a microstructured reactor," Appl. Catal. A **380**, 15–20 (2010).

[12] N. Iwasa, T. Mayanagi, S. Masuda, and N. Takezawa, "Steam reforming of methanol over Pd-Zn catalysts," React. Kinet. Catal. Lett. **69**, 355 (2000).

[13] C. Rameshan, H. Lorenz, L. Mayr, S. Penner, D. Zemlyanov, R. Arrigo, M. Haevecker, R. Blume, A. Knop-Gericke, R. Schlögl, and B. Klötzer, "CO_2-selective methanol steam reforming on In-doped Pd studied by *in situ* x-ray photoelectron spectroscopy," J. Catal. **295**, 186–194 (2012).

[14] Z.-X. Chen, K. M. Neyman, A. B. Gordienko, and N. Rösch, "Surface structure and stability of PdZn and PtZn alloys: Density-functional slab model studies," Phys. Rev. B **68**, 075417 (2003).

[15] U. Bardi, "The atomic structure of surface alloys and alloys surfaces," Rep. Prog. Phys. **57**, 939–987 (1994).

[16] A. Bayer, K. Flechtner, R. Denecke, H. P. Steinruck, K. M. Neyman, and N. Rosch, "Electronic properties of thin Zn layers on Pd(111) during growth and alloying," Surf. Sci. **600**, 78–94 (2006).

[17] G. Weirum, M. Kratzer, H. P. Koch, A. Tamtögl, J. Killmann, I. Bako, A. Winkler, S. Surnev, and R. Schennach, "Growth and desorption kinetics of ultrathin Zn layers on Pd(111)," J. Phys. Chem. C **113**, 9788–9796 (2009).

[18] X. He, Y. Huang, and Z.-X. Chen, "Zinc coverage dependent structure of PdZn surface alloy," Phys. Chem. Chem. Phys. **13**, 107–109 (2011).

[19] A. Benali, "Étude *ab initio* d'alliages AlCu: phénomènes de ségrégation et modification de la réactivité de surface vis-à-vis de l'oxygène," Ph.D. thesis, École doctorale Science de la Matière, Toulouse, 2010.

[20] D. Rouxel and B. Weber, "Surface des solides-physisorption-chimisorption-ségrégation," available online at http://www.techniques-ingenieur.fr/base-documentaire/sciences-fondamentales-th8/etats-de-la-matiere-42109210/surface-des-solides-af3680/.

[21] G. Tréglia, B. Legrand, F. Ducastelle, A. Saul, C. Gallis, I. Meunier, C. Mottet, and A. Senhaji, "Alloy surfaces: Segregation, reconstruction and phase transitions," Comput. Mater. Sci. **15**, 196–235 (1999).

[22] H. Kwak, Y. K. Shin, A. C. T. van Duin, and A. V. Vasenkov, "*Ab initio* based multiscale modeling of alloy surface segregation," J. Phys.: Condens. Matter **24**, 485006 (2012).

[23] G. McGuirk, J. Ledieu, É. Gaudry, M.-C. de Weerd, and V. Fournée, "Surface structures of Pd–In intermetallic compounds. I. Experimental study of structure and alloying of In thin films on Pd(111)," J. Chem. Phys. **141**, 084702 (2014).

[24] G. Kresse and J. Furthmüller, "Efficient iterative schemes for *ab initio* total-energy calculations using a plane-wave basis set," Phys. Rev. B **54**, 11169–11186 (1996).

[25] G. Kresse and J. Furthmüller, "Efficiency of *ab-initio* total energy calculations for metals and semiconductors using a plane wave basis set," Comput. Mater. Sci. **6**, 15–50 (1996).

[26] P. E. Blöchl, "Projector augmented-wave method," Phys. Rev. B **50**, 17953 (1994).

[27] G. Kresse and D. Joubert, "From ultrasoft pseudopotentials to the projector augmented-wave method," Phys. Rev. B **59**, 1758 (1999).

[28] J. P. Perdew, K. Burke, and M. Ernzerhof, "Generalized gradient approximation made simple," Phys. Rev. Lett. **77**, 3865 (1996).

[29] J. P. Perdew, K. Burke, and M. Ernzerhof, "Erratum: Generalized gradient approximation made simple," Phys. Rev. Lett. **78**, 1396 (1997).

[30] J. C. Boettger, "Nonconvergence of surface energies obtained from thin-film calculations," Phys. Rev. B **49**, 16798–16800 (1994).

[31] J. C. Boettger, J. R. Smith, U. Birkenheuer, N. Rösch, S. B. Trickey, R. Sabin, and S. P. Apell, "Extracting convergent surface formation energies from slab calculations," J. Phys.: Condens. Matter **10**, 893 (1998).

32J. L. F. Da Silva, C. Stampfl, and M. Scheffler, "Converged properties of clean metal surfaces by all-electron first principles calculations," Surf. Sci. **600**, 703–715 (2006).

33C. Jiang, L.-Q. Chen, and Z.-K. Liu, "First-principles study of constitutional and thermal point defects in b2 PdIn," Intermetallics **14**, 248–254 (2006).

34D. S. dos Santos, S. Miraglia, and D. Fruchart, "A high pressure investigation of Pd and the Pd-H system," J. Alloys Comp. **291**, L1–L5 (1999).

35C. Kittel, *Introduction to Solid State Physics*, 7th ed. (John Wiley and Sons, USA, 1996).

36Y. Zhang, "First-principles statistical mechanics approach to step decoration at solid surfaces," Ph.D. thesis, Freie Universität Berlin, 2008.

37H. Flandorfer, "Phase relationships in the in-rich part of the In-Pd system," J. Alloys Comp. **336**, 176–180 (2002).

38M. Giovannini, A. Saccone, S. Delfino, and P. Rogl, "A comparative investigation of isothermal sections of Rare Earth-Pd-In systems," Intermetallics **11**, 1237–1243 (2003).

39S. V. Meschel and O. J. Kleppa, "Standard enthalpies of formation of some transition metal indium compounds by high temperature direct synthesis calorimetry," J. Alloys Comp. **333**, 91–98 (2002).

40S. Amore, S. Delsante, N. Parodi, and G. Borzone, "Thermochemistry of Pd-In, Pd-Sn and Pd-Zn alloy systems," Thermochim. Acta **481**, 1–6 (2009).

41H. Kohlmann and C. Ritter, "Refinement of the crystal structures of palladium-rich In-Pd compounds by x-ray and neutron powder diffraction," Z. Naturforsch. B **62**, 929–934 (2007).

42M. Mansfield and R. J. Needs, "Surface energy and stress of lead (111) and (110) surfaces," Phys. Rev. B **43**, 8829–8833 (1991).

43P. J. Feibelman, "First-principles calculation of the geometric and electronic structure of the Be(0001) surface," Phys. Rev. B **46**, 2532–2539 (1992).

44A. Benali, C. Lacaze-Dufaure, and J. Morillo, "Density functional study of copper segregation in aluminum," Surf. Sci. **605**, 341–350 (2011).

45F. R. De Boer, R. Boom, W. C. M. Mattens, A. R. Miedema, and A. K. Niessen, *Cohesion in Metals* (Elsevier, Amsterdam, 1988).

46A. Michaelidis and M. Scheffler, "Introduction to the theory of metal surfaces," *Surface and Interface Science. Volume 1: Concepts and Methods*, edited by K. Wandelt (Wiley, 2012).

47L. Hammer, V. Blum, Ch. Schmidt, O. Wieckhorst, W. Meier, S. Müller, and K. Heinz, "Role of Co antisite segregation in the CoAl(111) surface," Phys. Rev. B **71**, 075413 (2005).

48V. Blum, L. Hammer, Ch. Schmidt, O. Wieckhorst, S. Müller, and K. Heinz, "Segregation in strongly ordering compounds: A key role of constitutional defects," Phys. Rev. Lett. **89**, 266102 (2002).

49A. V. Ruban, "Surface composition of ordered alloys: An off-stoichiometric effect," Phys. Rev. B **65**, 174201 (2002).

50A. Christensen, A. V. Ruban, P. Stoltze, K. W. Jacobsen, H. L. Skriver, J. K. Norskov, and F. Besenbacher, "Phase diagrams for surface alloys," Phys. Rev. B **56**, 5822–5834 (1997).

51K. Yuge, A. Seko, A. Kuwabara, F. Oba, and I. Tanaka, "Ordering and segregation of a $Cu_{75}Pt_{25}$(111) surface: A first-principles cluster expansion study," Phys. Rev. B **76**, 045407 (2007).

52O. K. Andersen, W. Klose, and H. Nohl, "Electronic structure of chevrel-phase high-critical-field superconductors," Phys. Rev. B **17**, 1209–1237 (1978).

53*Theory of Alloy Phase Formation*, in *Proceedings of the TMS-AIME Alloy Phases Committee and the Chemistry and Physics of Metals Committee at the 108th AIME Annual Meeting, New Orleans, USA, 19–20 February 1980*, edited by L. H. Bennett (Metallurgical Society of AIME, Warrendale, PA, 1980).

54Z.-X. Chen, K. M. Neyman, and N. Rösch, "Theoretical study of segregation of Zn and Pd in Pd-In alloys," Surf. Sci. **548**, 291–300 (2004).

55J. R. Kitchin, K. Reuter, and M. Scheffler, "Alloy surface segregation in reactive environments: First-principles atomistic thermodynamics study of Ag_3Pd(111) in oxygen atmospheres," Phys. Rev. B **77**, 075437 (2008).

56S. Piccinin, C. Stampfl, and M. Scheffler, "Ag-Cu alloy surfaces in an oxidizing environment: A first-principles study," Surf. Sci. **603**, 1467–1475 (2009).

57B. C. Han, A. Van der Ven, G. Ceder, and B. J. Hwang, "Surface segregation and ordering of alloy surfaces in the presence of adsorbates," Phys. Rev. B **72**, 205409 (2005).

58H. P. Koch, I. Bako, G. Weirum, M. Kratzer, and R. Schennach, "A theoretical study of Zn adsorption and desorption on a Pd(111) substrate," Surf. Sci. **604**, 926–931 (2010).